HHS Public Access

Author manuscript

Biochem Biophys Res Commun. Author manuscript; available in PMC 2020 June 30.

Published in final edited form as:

Biochem Biophys Res Commun. 2019 June 30; 514(3): 974–978. doi:10.1016/j.bbrc.2019.05.064.

Structural studies of antiviral inhibitor with HIV-1 protease bearing drug resistant substitutions of V32I, I47V and V82I

Shrikant Pawar[a,b], **Yuan-Fang Wang**[a], **Andres Wong-Sam**[a], **Johnson Agniswamy**[a], **Arun K. Ghosh**[c], **Robert W. Harrison**[a,b], and **Irene T. Weber**[a,*]

[a]Department of Biology, Georgia State University, Atlanta, GA, 30303, USA

[b]Department of Computer Science, Georgia State University, Atlanta, GA, 30303, USA

[c]Department of Chemistry and Department of Medicinal Chemistry and Molecular Pharmacology, Purdue University, West Lafayette, IN, 47907, USA

Abstract

HIV-1 protease inhibitors are effective in HIV/AIDS therapy, although drug resistance is a severe problem. This study examines the effects of four investigational inhibitors against HIV-1 protease with drug resistant mutations of V32I, I47V and V82I (PR_{Tri}) that model the inhibitor-binding site of HIV-2 protease. These inhibitors contain diverse chemical modifications on the darunavir scaffold and form new interactions with wild type protease, however, the measured inhibition constants for PR_{Tri} mutant range from 17 to 40 nM or significantly worse than picomolar values reported for wild type enzyme. The X-ray crystal structure of PR_{Tri} mutant in complex with inhibitor 1 at 1.5 Å resolution shows minor changes in interactions with inhibitor compared with the corresponding wild type PR complex. Instead, the basic amine at P2 of inhibitor together with mutation V82I induces two alternate conformations for the side chain of Arg8 with new interactions with inhibitor and Leu10. Hence, inhibition is influenced by small coordinated changes in hydrophobic interactions.

Keywords

HIV-1 protease; Antiviral inhibitors; Drug resistance; X-ray crystallography

1. Introduction

HIV/AIDS is a pandemic disease with about 37 million people infected worldwide [1]. HIV infection can be controlled by antiviral drugs targeting different stages of viral replication, however, the genetic diversity of the virus and rapid selection of drug resistant strains pose a severe challenge [2,3]. The retrovirus HIV includes two types, HIV-1 and HIV-2, and HIV-1 is subdivided into three groups (M, O, and N) and subtypes with different geographical

*Corresponding author. iweber@gsu.edu (I.T. Weber).

Conflicts of interest

None declared.

Transparency document

Transparency document related to this article can be found online at https://doi.org/10.1016/j.bbrc.2019.05.064.

distribution. HIV-2 infections are common in West Africa, however, some drugs designed for HIV-1 are not effective for HIV-2 infections [4].

One important class of antiviral drugs targets the viral protease (PR), which is crucial for production of infectious virus. PR processes cleavage sites in Gag-Pol region during viral maturation to produce individual structural proteins [5]. This aspartic protease is catalytically active as a dimer of 99-residue monomers [6]. Clinical inhibitors bind in the active site cavity of the enzyme and block binding of substrates. Some HIV-1 PR inhibitors, including amprenavir (APV), are significantly less potent against HIV-2 infections probably because the amino acid sequences of HIV-1 and HIV-2 PRs show only about 40% sequence identity [7]. In addition to its natural genetic diversity, the virus has evolved resistance mutations for all clinical protease inhibitors (PIs) [8]. Single, major mutations decrease binding of inhibitor, however, they can be deleterious for viral replication. Resistance mutations can alter the catalytic activity, binding affinity and stability of PR [9,10]. The virus evolves additional mutations that compensate by restoring effective viral replication in the presence of inhibitor [11].

HIV-1 PR with drug resistant mutations V32I, I47V and V82I (PR_{Tri}) has been evaluated as a model for inhibition of HIV-2 PR to overcome the problem of autoproteolysis of HIV-2 PR. The three mutations in PR_{Tri} alter residues in the inhibitor-binding cavity (Fig. 1A) and represent the changes in the inhibitor binding site of HIV-2 protease. APV showed poor inhibition of both PR_{Tri} and HIV-2 PR at 15- and 19-fold worse than for HIV-1 PR, while darunavir (DRV) and saquinavir (SQV) were effective inhibitors of all three enzymes [12]. Moreover, the individual mutations of V32I, I47V and V82I are associated with resistance to one or more clinical inhibitors [8]. Hence, PR_{Tri} was chosen to evaluate the ef-ficacy of investigational inhibitors for drug-resistant mutants and HIV-2 PR.

The four investigational antiviral inhibitors were designed on the DRV scaffold (Fig. 1B) with the aim of introducing new interactions of the P2 group with PR. They exhibited potent antiviral activity on wild type and drug resistant strains of HIV-1. Crystal structures confirmed the presence of new interactions of wild type PR with the P2 groups of these inhibitors compared to DRV. Inhibitor **1** has a novel P2 bis-THF group with a basic amine that forms direct and water-mediated hydrogen bond interactions with the main chain carbonyl oxygen and amide of Gly48 in the PR flap [13]. Inhibitor **2** contains *tris*-tetrahydrofuranylurethane (*tris*-THF) as the P2 ligand instead of *bis*-THF in DRV [14–16]. The third THF group introduces new water-mediated hydrogen bond interactions with Gly27 and Arg87 in the PR dimer interface. Inhibitor **3** has a novel tricycle cyclohexyl-bis-tetrahydrofuranylurethane at P2, and resembles inhibitor **2** in its new water-mediated interactions [17]. This inhibitor showed favorable penetration of the central nervous system (CNS) in an in vitro model [18]. Inhibitor **4** has a 3-(S)eN-methoxycarbonyl amino substituted cyclopentyltetrahydrofuranyl (Cp-THF) at the P2 group [19]. The carbamate NH of the ligand forms hydrogen bonds with the main chain of Gly48 similar to those of inhibitor **1** and the carbamate carbonyl has a water-mediated interaction with the guanidinium group of Arg8. Therefore, we hypothesized they would show good inhibition of PR_{Tri}. Inhibition constants were measured for the four compounds, and a high resolution X-ray structure was determined for PR_{Tri} in complex with inhibitor **1**.

2. Materials and methods

2.1. Inhibitors

Amprenavir (APV) (HPLC purity of 99.7%) was obtained from the AIDS Reagent Program, Division of AIDS, NIAID, NIH. Compounds **1–4** (>95.0% purity by HPLC) were provided by Dr. Arun Ghosh at Purdue University.

2.2. Protein purification

The clone for triple mutant PR_{Tri} (V32I, I47V and V82I) includes optimizing mutations of Q7K, L33I, and L63I to decrease autoproteolysis, and C67A, C95A to eliminate cysteine-thiol oxidation [20]. Protein was expressed in *E. coli* BL21 and purified from inclusion bodies as described previously [21,22] using gel filtration followed by reverse phase chromatography and refolding. Samples were concentrated to 5.0 mg/mL for crystallization or diluted for kinetic assays.

2.3. Protein crystallography

PR_{Tri} was mixed with inhibitor (dissolved in dimethylsulfoxide) at a molar ratio of 1:5. Crystals were grown at room temperature by hanging drop vapor diffusion. Each drop contained 1 mL protein and 1 mL reservoir solution. Crystals of PR_{Tri} in complex with compound **1** were grown from 0.1 M sodium acetate, pH 4.6, and 2 M NaCl. Crystals were cryo-protected in 30% glycerol and flash frozen in liquid nitrogen. X-ray diffraction data were collected on the SERCAT 22BM beamline, Advanced Photon Source, Argonne National Laboratory (Argonne, IL), and processed using HKL-2000 [23]. The structure was solved by molecular replacement with PR complex with APV (3NU3) [24] using CCP4i Phaser [25,26]. The structure was refined with SHELX-2014 [27], followed by REFMAC5 [28]. COOT [29] was used for visualization and refitting. Alternate conformations were modeled according to the electron density maps. Anisotropic B factors were applied in the refinement. Structural figures were made using PyMOL [30]. Atomic coordinates and structure factors for PR_{Tri}/**1** have been deposited in the PDB [31] with ID: 6OTG.

2.4. Enzyme kinetic assays

Kinetic parameters of PR_{Tri} were determined in 3e5 replicate runs by monitoring hydrolysis of fluorescence substrate derived from the HIV-1 p2/NC cleavage site: Abz-Thr-Ile-Nle-*p*-nitro-Phe-Gln-Arg-NH_2 (BACHEM H-2992) (where Abz is anthranilic acid, Nle is norleucine, and *p*-nitro-Phe is *p*-nitrophenylalanine). Samples were equilibrated at 37 °C for 5 min prior to initiating the reactions. Enzyme activity was measured at 37 °C using a PolarStar Optima microplate reader (BMG Labtech) with excitation wavelength at 340 nm and emission wavelength at 420 nm, as described previously [24,32]. To determine catalytic efficiency, 10 μL of PR_{Tri} (final well concentration of 40–100 nM determined by active site titration with APV) was mixed with 100 μL reaction buffer (100 mMMES pH 5.6, 400 mM NaCl, 1 mM EDTA, and 5% glycerol). Reaction was initiated by adding 100 μL substrate (12–96 μM final concentration). Initial velocities (V_0) were determined using MARS software (BMG Labtech). The K_m and k_{cat} were determined by fitting data to the Michaelis-Menten plot of V_0 vs [substrate].

For inhibition studies, 10 μL PR_{Tri} was mixed with 98 μL reaction buffer and 2 μL inhibitor in DMSO (final well concentration 0–40 mM). Reaction was initiated with 90 μL substrate (final well concentration 60 mM). IC_{50} values were determined using Sigma-Plot (Systat Software) by non-linear regression curve fitting to a dose-response plot of V_0 vs [inhibitor]. K_i values were calculated using the equation for tight-binding inhibitor of K_i= (IC_{50} - 0.5[E])/ (1 þ [S]/K_m) [33].

For the urea denaturation assay, 10 mL PR_{Tri} was mixed with 100 mL reaction buffer containing 8 different urea concentrations (0–4 μM). Reaction was initiated with 90 μL substrate (final well concentration 60–72 μM) in 0–4 M urea. The urea concentration in each well remained the same throughout the experiment. A plot of V_0 vs [urea] was constructed using SigmaPlot (Systat Software) and sigmoidal curve fitting used to determine the urea concentration for 50% maximum velocity (UC_{50}).

3. Results

3.1. Kinetic parameters, inhibition and stability of PR_{Tri} mutant

Kinetic parameters were determined for PR_{Tri} hydrolysis of a fluorescent substrate analog at 37 °C prior to assaying the effects of compounds **1–4** under the same conditions. PR_{Tri} mutant had k_{cat} of 299 ± 48 μM/min and K_m of 72 ± 17.7 μM. The catalytic efficiency (k_{cat} /K_m) of 4.2 μM^{-1} min^{1} is similar to that value of 6.5 μM^{1} min^{1} for wild type enzyme at 26° C [34].

The measured K_i values were 31.4 ± 3.9 nM for compound **1**, 38.4 ± 1.2 nM for compound **2**, 16.7 ± 0.8 nM for compound **3**, and 39.5 ± 6.1 nM for compound **4**. These K_i values were significantly worse for the mutant compared to K_i values of 2 to 10 pM reported for the wild type enzyme [13,15,17,19]. Therefore, these antiviral inhibitors are unlikely to be effective on HIV-1 with these mutations or on HIV-2.

The stability of the mutant and wild type proteases were assessed by measuring enzyme activity under urea denaturation. A UC_{50} value of 0.97 ± 0.05 M was obtained for PR_{Tri} mutant. In comparison, the wild type enzyme gave a UC_{50} value of 0.70 ± 0.07 M under the same conditions. These values suggest the mutant dimer is somewhat more stable than the wild type protease.

3.2. Crystallographic analysis of PR_{Tri} complex with inhibitor 1

Co-crystallization experiments were performed for the four compounds, however, crystals grew only for PR_{Tri} with compound **1**. The crystal structure of PR_{Tri}/**1** was solved at 1.50 Å resolution in the $P2_12_12$ space group, and refined to R/R_{free} values of 13.4/17.2%. Crystallographic statistics are listed in Table 1. The asymmetric unit of the crystal structure contained a dimer of PR_{Tri}, and the inhibitor was bound at the active site in two alternate orientations with an occupancy ratio of 0.5/0.5. The solvent was modeled with 133 water, 1 glycerol and 4 formic acid molecules from the crystallization and cryo-protectant solutions. The crystal structure of PR_{Tri}/**1** was compared with the corresponding complex of wild type PR (PDB ID: 5BRY), which was determined at 1.34 Å resolution in the same space group with isomorphous unit cell dimensions and contained PR dimer with inhibitor bound in two

orientations with 0.6/0.4 relative occupancy [13]. The two dimer structures superimposed with a low RMSD value of 0.23 Å on Cα atoms.

The interactions of PR_{Tri} with inhibitor were analyzed in comparison to those in wild type PR complex. Inhibitor **1** forms six direct hydrogen bonds with PR_{Tri}, excluding the interactions of the central hydroxyl with the catalytic Asp25 and 25' (Fig. 2). Additionally, it forms water-mediated interactions with flap residues Gly48, Ile50 and Ile50', while one orientation of inhibitor (designated as the "major" conformation) has a water-mediated interaction with the carboxylate side chain of Asp29. PR-inhibitor hydrogen bond interactions are conserved in the mutant and wild type complexes with differences of no greater than 0.2 Å in length for the major inhibitor conformations. This inhibitor was designed to incorporate an amine on *bis*-THF at P2 that forms a new direct hydrogen bond interaction with the carbonyl oxygen of Gly48, a water-mediated interaction with the amide of Gly48 in the flap region, and a second water-mediated interaction with the side chain of Asp29. These interactions of compound **1** cannot occur with clinical inhibitor DRV, which lacks the basic amine. However, the minor conformation of **1** in PR_{Tri} complex has lost the second water and its interaction with Asp29.

The hydrophobic side chains of residues 32, 47 and 82 are important components of the PR binding site for substrates or inhibitors. In wild type PR/**1,** Val82 interacts with the P1 and P1' groups of inhibitors, while Val32 and Ile47 contribute to the binding site for P2 and P2' groups. Ile82 in the mutant has similar interactions with inhibitor P1 and P1' as seen for Val82 of wild type enzyme. Val32 and Ile32 show similar van der Waals contacts with the P2 group of **1**, while Val47 in the mutant has shifted to form new interactions with P2 compared to Ile47 in the flap. The P2' group has gained van der Waals interactions with Ile32' and lost contacts with Val47' relative to those in the wild type structure.

In addition to the contacts with inhibitors, these residues interact with adjacent PR side chains. The side chains of residue 32 and 47 form hydrophobic contacts with each other and with neighboring side chains of Asp30, Lys45, Ile54, Val56, Leu76, Thr80, Ile84 and Ile50' (Fig. 3). The majority of these internal hydrophobic contacts are retained in the PR_{Tri} mutant. The most significant change is a shift of about 0.5 Å in the Ca atoms of both Val47 and 47' relative to their locations in wild type PR. This change is illustrated in Fig. 3 for Val47/Ile47. This shift enables Val47 to form 3 new hydrophobic contacts with the P2 group of inhibitor, while losing contacts with neighboring side chains of Asp30, Lys45, Ile54 and Ile50'.

Mutation of Val82 to the longer Ile introduces new van der Waals interactions and significant changes in the side chain conformation of Arg8. In the wild type PR complex, the side chain of Arg8 has a single conformation that forms a key intersubunit ion pair with Asp29' and no contacts with inhibitor. In the PR_{Tri}/**1** structure, the longer side chain of Ile82/82' appears to induce two alternate conformations of Arg8/8' with equivalent changes in both subunits (Fig. 4A). The guanidinium group of one conformation of Arg8 retains the ion pair with Asp29' and also forms a new van der Waals contact with the P2 group of inhibitor. The second conformation of Arg8 is rotated away to form van der Waals contacts with Leu10 instead of the intersubunit ionic interaction with Asp29'. The second conformation of Arg8/8' is not

observed in the corresponding complex of PR_{Tri}/DRV, probably because DRV lacks the extra amine of compound **1** (Fig. 4B). These changes may be due to the local environment, since a multiple mutant PR20 has similar alternative conformations of Arg8/8' related to the substitution of the larger Phe side chain instead of Leu10 [35].

4. Discussion

The four tested investigational antiviral compounds were poor inhibitors (K_i values of 16.7–39.5 nM) of HIV-1 PR_{Tri} despite their excellent pM inhibition of wild type enzyme [13,15,17,19]. Analysis of protease-inhibitor interactions in the crystal structure of PR_{Tri}/**1** revealed the loss of one water-mediated polar interaction in one orientation of inhibitor and small changes in hydrophobic contacts. In particular, Val47 loses hydrophobic contacts with flap residues Lys45, Ile50' and Ile54 compared to those of wild type complex. The most substantial change compared to the wild type complex occurred for mutated residue Ile82/82', where the larger side chain produces two alternate conformations for the side chain of Arg8/8'. One conformation of the guanidinium group of Arg8/8' forms new van der Waals contacts with Leu10 and the P2 group of inhibitor **1** instead of its typical intersubunit ion pair with Asp29'/29. We previously reported the crystal structures of PR_{Tri} complexes with APV, DRV and SQV [12]. These structures exhibited a single conformation for Arg8/8', except for the APV complex which had two alternate conformations for Arg8' side chain in one subunit and new van der Waals contacts with Ile82' and Leu10' similar to those seen in the PR_{Tri}/**1** structure. Moreover, only a single conformation was observed for Arg8/8' in our structures of HIV-2 PR with different inhibitors [12,36]. This change in conformation seen for Arg8/8' in PR_{Tri}/**1**, comprising partial loss of its intersubunit ion pair and new intra-subunit interactions, might be expected to alter the stability of the mutant, however, the UC50 for urea denaturation remains close to the value for wild type PR. In contrast, PR mutant with the single substitution of R8Q, which completely eliminated the ion pair with Asp29', showed decreased stability with UC_{50} of 0.7 relative to wild type enzyme [37]. Overall, the loss of internal contacts among flap residues and disruption of the ion pair between Arg8 and Asp29' are consistent with molecular dynamics simulations suggesting substitutions V32I, I47V and V82I in HIV-2 PR decrease the hydrophobic interactions with APV and DRV [38].

This new structure of PR_{Tri}/**1** suggests how drug resistant mutations of V32I and I47V on opposite sides of the S2 and S2' subsites can partially compensate for altered hydrophobic interactions with inhibitors and other protease residues, while mutation V82I induces alternate conformations of Arg8/8' and introduces new interactions with Leu10 and the P2 group of 1. Structural analysis suggests these changes in hydrophobic interactions are specific for this combination of compound **1** and mutant PR_{Tri} and act to decrease the inhibition.

Supplementary Material

Refer to Web version on PubMed Central for supplementary material.

Acknowledgements

We thank the staff at the Southeast Regional-Collaborative Access Team (SER-CAT) at the Advanced Photon Source, Argonne National Laboratory, for assistance during X-ray data collection. Supporting institutions may be found at http://www.ser-cat.org/members.html. Use of the Advanced Photon Source was supported by the U.S. Department of Energy, Office of Science, Office of Basic Energy Sciences, under Contract No. W-31–109-Eng-38.

Funding

This research was supported by the National Institutes of Health grant GM062920 and a Georgia State University Molecular Basis of Disease fellowship. Design and synthesis of the compounds was supported by National Institutes of Health grant GM53386.

References

[1]. World Health Organization. http://www.who.int/mediacentre/factsheets/fs360/en/,, 2016 4 2019.

[2]. Hemelaar J, Implications of HIV diversity for the HIV-1 pandemic, J. Infect 66 (2013) 391–400. 10.1016/j.jinf.2012.10.026. [PubMed: 23103289]

[3]. Clutter DS, Jordan MR, Bertagnolio S, Shafer RW, HIV-1 drug resistance and resistance testing, Infect. Genet. Evol 46 (2016) 292–307. 10.1016/j.meegid.2016.08.031. [PubMed: 27587334]

[4]. Menendez-Arias L, Alvarez M, Antiretroviral therapy and drug resistance in human immunodeficiency virus type 2 infection, Antivir. Res 102 (2014) 70–86. 10.1016/j.antiviral.2013.12.001. [PubMed: 24345729]

[5]. Konvalinka J, Krausslich HG, Muller B, Retroviral proteases and their roles in virion maturation, Virology 479–480 (2015) 403–417. 10.1016/j.virol.2015.03.021.

[6]. Tang C, Louis JM, Aniana A, Suh JY, Clore GM, Visualizing transient events in amino-terminal autoprocessing of HIV-1 protease, Nature 455 (2008) 693–696. 10.1038/nature07342. [PubMed: 18833280]

[7]. Menendez-Arias L, Tozser J, HIV-1 protease inhibitors: effects on HIV-2 replication and resistance, Trends Pharmacol. Sci 29 (2008) 42–49.10.1016/j.tips.2007.10.013. [PubMed: 18054799]

[8]. Wensing AM, Calvez V, Gunthard HF, et al., Update of the drug resistance mutations in HIV-1, Top Antivir. Med 24 (2017) 132–133, 2017, https://www.ncbi.nlm.nih.gov/pmc/articles/PMC5677049/pdf/tam-24-132.pdf. [PubMed: 28208121]

[9]. Menendez-Arias L, Molecular basis of human immunodeficiency virus type 1 drug resistance: overview and recent developments, Antivir. Res 98 (2013) 93–120. 10.1016/j.antiviral.2013.01.007. [PubMed: 23403210]

[10]. Weber IT, Agniswamy J, HIV-1 protease: structural perspectives on drug resistance, Viruses 1 (2009) 1110–1136. 10.3390/v1031110. [PubMed: 21994585]

[11]. Nijhuis M, Schuurman R, de Jong D, et al., Increased fitness of drug resistant HIV-1 protease as a result of acquisition of compensatory mutations during suboptimal therapy, AIDS 13 (1999) 2349–2359. [PubMed: 10597776]

[12]. Tie Y, Wang YF, Boross PI, et al., Critical differences in HIV-1 and HIV-2 protease specificity for clinical inhibitors, Protein Sci. 21 (2012) 339–350. 10.1002/pro.2019. [PubMed: 22238126]

[13]. Ghosh AK, Martyr CD, Osswald HL, et al., Design of HIV-1 protease inhibitors with amino-bis-tetrahydrofuran derivatives as P2-ligands to enhance backbone-binding interactions: synthesis, biological evaluation, and protein-ligand X-ray studies, J. Med. Chem 58 (2015) 6994–7006. 10.1021/acs.jmedchem.5b00900. [PubMed: 26306007]

[14]. Zhang H, Wang YF, Shen CH, et al., Novel P2 tris-tetrahydrofuran group in antiviral compound 1 (GRL-0519) fills the S2 binding pocket of selected mutants of HIV-1 protease, J. Med. Chem 56 (2013) 1074–1083. 10.1021/jm301519z. [PubMed: 23298236]

[15]. Ghosh AK, Xu CX, Rao KV, et al., Probing multidrug-resistance and protein-ligand interactions with oxatricyclic designed ligands in HIV-1 protease inhibitors, ChemMedChem 5 (2010) 1850–1854. 10.1002/cmdc.201000318. [PubMed: 20827746]

[16]. Amano M, Tojo Y, Salcedo-Gomez PM, et al., GRL-0519, a novel oxatricyclic ligand-containing nonpeptidic HIV-1 protease inhibitor (PI), potently suppresses replication of a wide spectrum of multi-PI-resistant HIV-1 variants in vitro, Antimicrob. Agents Chemother 57 (2013) 2036–2046. 10.1128/AAC.02189-12. [PubMed: 23403426]

[17]. Ghosh AK, Parham GL, Martyr CD, et al., Highly potent HIV-1 protease inhibitors with novel tricyclic P2 ligands: design, synthesis, and protein-ligand X-ray studies, J. Med. Chem 56 (2013) 6792–6802. 10.1021/jm400768f. [PubMed: 23947685]

[18]. Amano M, Tojo Y, Salcedo-Gomez PM, et al., A novel tricyclic ligand-containing nonpeptidic HIV-1 protease inhibitor, GRL-0739, effectively inhibits the replication of multidrug-resistant HIV-1 variants and has a desirable central nervous system penetration property in vitro, Antimicrob. Agents Chemother 59 (2015) 2625–2635. 10.1128/AAC.04757-14. [PubMed: 25691652]

[19]. Ghosh AK, Chapsal BD, Steffey M, et al., Substituent effects on P2-cyclopentyltetrahydrofuranyl urethanes: design, synthesis, and X-ray studies of potent HIV-1 protease inhibitors, Bioorg. Med. Chem. Lett 22 (2012) 2308–2311. 10.1016/j.bmcl.2012.01.061. [PubMed: 22364812]

[20]. Wondrak EM, Louis JM, Influence of flanking sequences on the dimer stability of human immunodeficiency virus type 1 protease, Biochemistry 35 (1996) 12957–12962. 10.1021/bi960984y. [PubMed: 8841142]

[21]. Sayer JM, Agniswamy J, Weber IT, Louis JM, Autocatalytic maturation, physical/chemical properties, and crystal structure of group N HIV-1 protease: relevance to drug resistance, Protein Sci 19 (2010) 2055–2072. 10.1002/pro.486. [PubMed: 20737578]

[22]. Louis JM, Ishima R, Aniana A, Sayer JM, Revealing the dimer dissociation and existence of a folded monomer of the mature HIV-2 protease, Protein Sci 18 (2009) 2442–2453. 10.1002/pro.261. [PubMed: 19798742]

[23]. Otwinowski Z, Minor W, Processing of X-ray diffraction data collected in oscillation mode, Methods Enzymol. 276 (1997) 307–326.

[24]. Shen CH, Wang YF, Kovalevsky AY, et al., Amprenavir complexes with HIV-1 protease and its drug-resistant mutants altering hydrophobic clusters, FEBS J. 277 (2010) 3699–3714. 10.1111/j.1742-4658.2010.07771.x. [PubMed: 20695887]

[25]. McCoy AJ, Grosse-Kunstleve RW, Adams PD, et al., Phaser crystallographic software, J. Appl. Crystallogr 40 (2007) 658–674. 10.1107/S0021889807021206. [PubMed: 19461840]

[26]. Winn MD, Ballard CC, Cowtan KD, et al., Overview of the CCP4 suite and current developments, Acta Crystallogr. Sect. D Biol. Crystallogr 67 (2011) 235–242. 10.1107/S0907444910045749. [PubMed: 21460441]

[27]. Sheldrick GM, Crystal structure refinement with SHELXL, Acta Crystallogr. C Struct. Chem 71 (2015) 3–8. 10.1107/S2053229614024218. [PubMed: 25567568]

[28]. Murshudov GN, Vagin AA, Dodson EJ, Refinement of macromolecular structures by the maximum-likelihood method, Acta Crystallogr. Sect. D Biol. Crystallogr 53 (1997) 240–255. 10.1107/S0907444996012255. [PubMed: 15299926]

[29]. Emsley P, Lohkamp B, Scott WG, Cowtan K, Features and development of coot, Acta Crystallogr. Sect. D Biol. Crystallogr 66 (2010) 486–501. 10.1107/S0907444910007493. [PubMed: 20383002]

[30]. DeLano WL, Pymol: an Open-Source Molecular Graphics Tool, CCP4 Newsletter on Protein Crystallography, 2002, pp. 82–92. https://www.ccp4.ac.uk/newsletters/newsletter40/11_pymol.pdf.

[31]. Berman HM, Westbrook J, Feng Z, et al., The protein data bank, Nucleic Acids Res. 28 (2000) 235–242. 10.1107/S0907444902003451. [PubMed: 10592235]

[32]. Wong-Sam A, Wang YF, Zhang Y, et al., Drug resistance mutation L76V alters nonpolar interactions at the flap-core interface of HIV-1 protease, ACS Omega 3 (2018) 12132–12140. 10.1021/acsomega.8b01683. [PubMed: 30288468]

[33]. Copeland RA, Lombardo D, Giannaras J, Decicco CP, Estimating K-I values for tight-binding inhibitors from dose-response plots, Bioorg. Med. Chem. Lett 5 (1995) 1947–1952. 10.1016/0960-894x(95)00330-V.

[34]. Liu F, Kovalevsky AY, Tie Y, et al., Effect of flap mutations on structure of HIV-1 protease and inhibition by saquinavir and darunavir, J. Mol. Biol 381 (2008) 102–115. 10.1016/j.jmb.2008.05.062. [PubMed: 18597780]

[35]. Agniswamy J, Shen CH, Aniana A, et al., HIV-1 protease with 20 mutations exhibits extreme resistance to clinical inhibitors through coordinated structural rearrangements, Biochemistry 51 (2012) 2819–2828. 10.1021/bi2018317. [PubMed: 22404139]

[36]. Kovalevsky AY, Louis JM, Aniana A, et al., Structural evidence for effectiveness of darunavir and two related antiviral inhibitors against HIV-2 pro-tease, J. Mol. Biol 384 (2008) 178–192. 10.1016/j.jmb.2008.09.031. [PubMed: 18834890]

[37]. Mahalingam B, Louis JM, Reed CC, et al., Structural and kinetic analysis of drug resistant mutants of HIV-1 protease, Eur. J. Biochem 263 (1999) 238–245. 10.1046/j.1432-1327.1999.00514.x. [PubMed: 10429209]

[38]. Chen J, Drug resistance mechanisms of three mutations V32I, I47V and V82I in HIV-1 protease toward inhibitors probed by molecular dynamics simulations and binding free energy predictions, RSC Adv. (2016) 58573–58585. 10.1039/C6RA09201B.

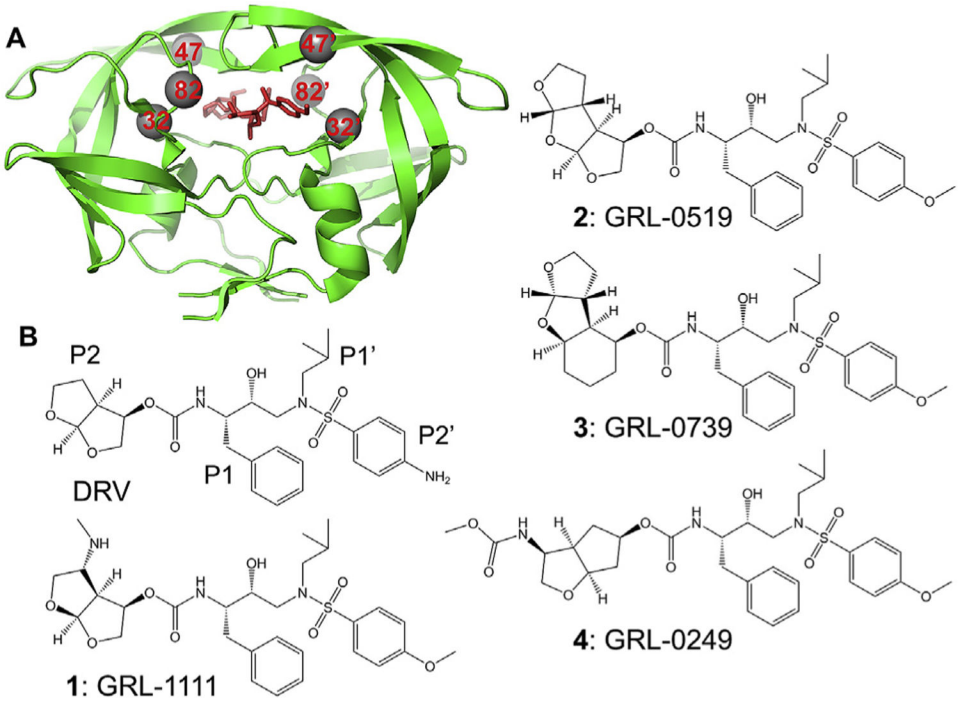

Fig. 1. HIV PR dimer with sites of mutations and selected inhibitors.

A) Sites of mutation in HIV-1 PR dimer with inhibitor GRL-1111. PR is shown as green ribbons with sites of the three mutations, V32I, I47V and V82I, indicated as grey spheres. Inhibitor is shown in red sticks.

B) Structures of darunavir and investigational inhibitors. The P2-P2' groups are indicated for DRV. (For interpretation of the references to colour in this figure legend, the reader is referred to the Web version of this article.)

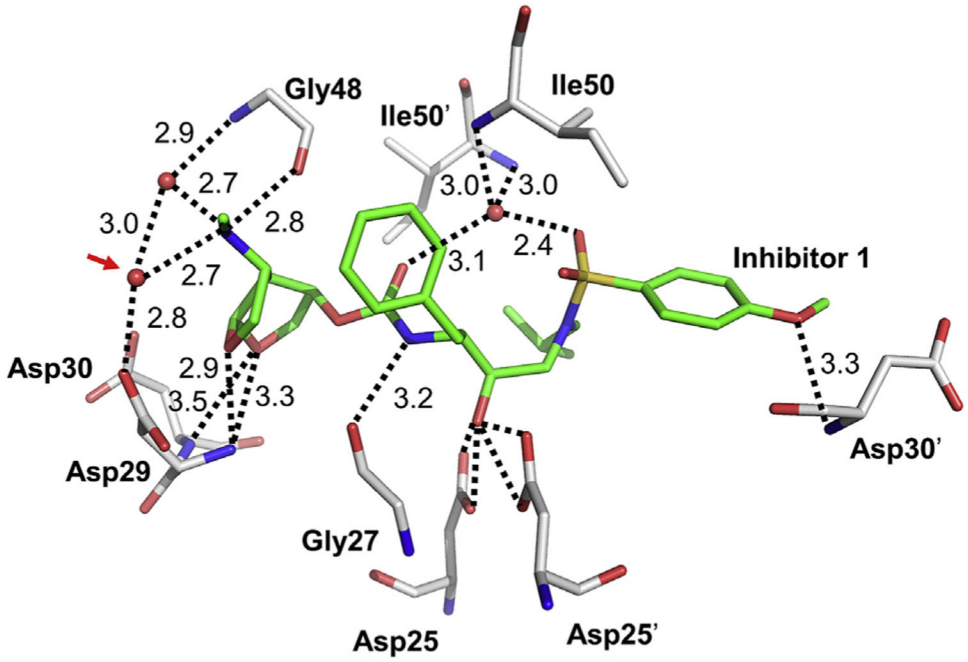

Fig. 2. Hydrogen bond interactions of PR_{Tri} with inhibitor 1.

Protein is shown as grey sticks and inhibitor in green sticks. Dotted lines indicate hydrogen bond interactions with interatomic distances in Å. (For interpretation of the references to colour in this figure legend, the reader is referred to the Web version of this article.)

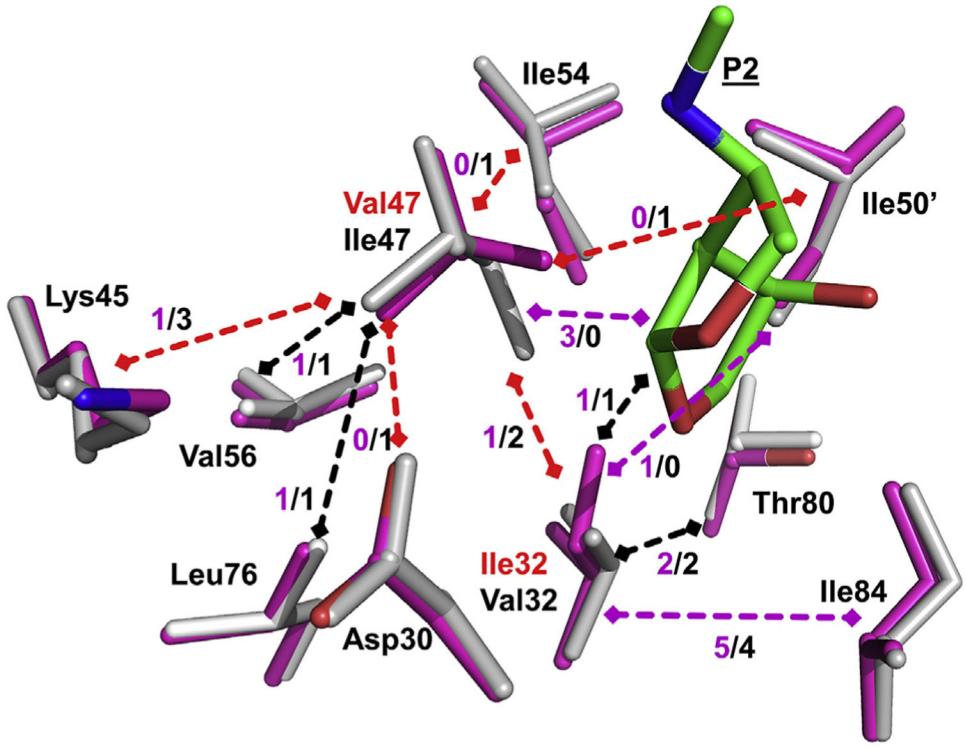

Fig. 3. Hydrophobic interactions of residues 32 and 47.

Residues in PR_{Tri} are shown in magenta sticks superimposed on corresponding residues of wild type PR in grey. Mutations Ile32 and Val47 are labeled in red, and P2 group of inhibitor is green. Hydrophobic interactions between residues are shown as dashed arrows with the number of contacts indicated. Black arrows indicate identical contacts in both structures, red arrows mark fewer contacts, and magenta arrows show more contacts in mutant than in wild type PR. (For interpretation of the references to colour in this figure legend, the reader is referred to the Web version of this article.)

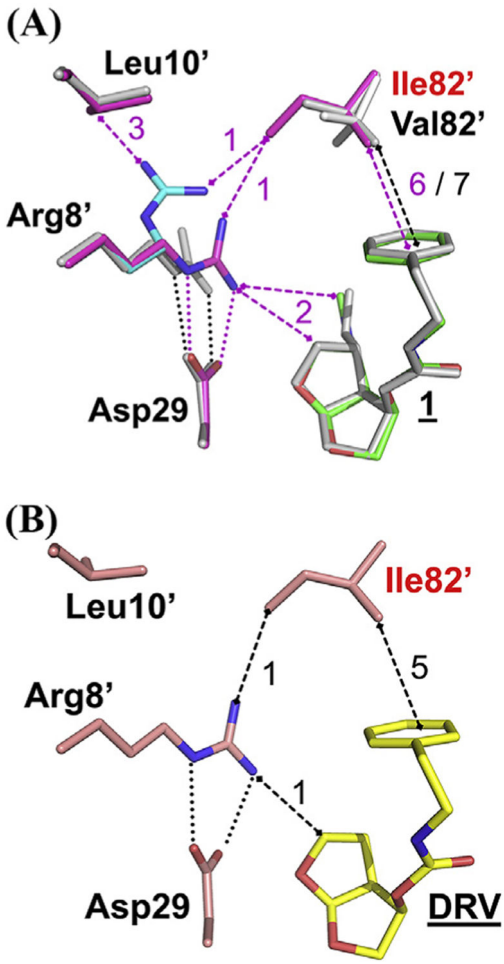

Fig. 4. Interactions of alternative conformations of Arg8′ with neighboring side chains and inhibitor.

A) Mutant PR_{Tri} is shown in magenta sticks with alternate conformation of Arg8′ in cyan and inhibitor **1** in green. Wild type PR and inhibitor are grey. Dotted lines indicate ionic interaction, and dashed lines indicate hydrophobic interactions. CH-p interactions with the aromatic P1 group of inhibitor are indicated by a single dashed line. B) Mutant PR_{Tri} in peach bonds with DRV in yellow sticks. (For interpretation of the references to colour in this figure legend, the reader is referred to the Web version of this article.)

Table 1

Crystallographic Data Collection and Refinement Statistics.

(Values in parentheses are given for the highest resolution shell.).

	PR_{Tri}/GRL-1111
Space group	$P2_12_12$
Unit cell dimensions: (Å)	
A	58.57
B	86.52
C	45.32
Resolution range (Final Shell)(Å)	50–1.50 (1.55–1.50)
Unique reflections	37,188 (2,865)
R_{merge} (%) overall (final shell)	5.9 (49.2)
I/σ(I) overall (final shell)	26.6 (3.1)
Completeness (%) overall (final shell)	96.8 (76.4)
Redundancy (final shell)	6.7 (4.1)
R (%)	13.4
R_{free} (%)	17.2
No. of solvent atoms	151
RMS deviation from ideality	
Bonds (Å)	0.020
Angle distance (degree)	2.29
Average B-factors (A^2)	
Wilson B-factor	17.7
Main-chain atoms	17.0
Side-chain atoms	23.6
Inhibitor	15.7
Solvent	28.3